

Rydberg-state reionization of multiply charged ions escaping from solid surfaces

Lj. D. Nedeljković and N. N. Nedeljković*

Faculty of Physics, University of Belgrade, P.O. Box 368, Belgrade, Yugoslavia

(Received 25 July 2002; revised manuscript received 15 November 2002; published 18 March 2003)

Reionization rates of Rydberg states ($n \gg 1$ and $l=0, 1$, and 2) of multiply charged ionic projectiles escaping solid surfaces are calculated. These rates are obtained in an analytic form as a function of the ion-surface distance R . A phenomenological model of the reionization process, based on two-state quantum dynamics, is adopted for the vicinity of the potential barrier top. The results of calculations show that ionization rates for different Rydberg states are strictly localized and relatively separated. Universality of the reionization rate as a function of the scaling parameter α , describing the turning point configurations, is demonstrated. The reionization is discussed within the framework of a nonresonant population-reionization process at intermediate ionic velocities ($v \sim 1$ a.u.). The influence of reionization on the population of ionic Rydberg states is expressed in terms of a renormalized neutralization rate. It is demonstrated that the reionization effect significantly changes the population curves for all Rydberg states. The population curves obtained correlate with beam-foil experimental data concerning the S VI, Cl VII, and Ar VIII ions.

DOI: 10.1103/PhysRevA.67.032709

PACS number(s): 34.50.Fa, 34.50.Dy, 79.20.Rf

I. INTRODUCTION

A number of valuable contributions to the theory of multiply charged ions ($Z \gg 1$) or Rydberg atoms ($n \gg 1$) interacting with solid surfaces are concentrated in the low velocity region of the projectiles ($v \ll 1$ a.u.).

In the last decade, the theoretical activity has developed in several different directions. The semiclassical over-barrier model [1,2] and its extended dynamical version [3,4] reflect global physical aspects of electron capture and recapture at low velocities. The quantum description, necessary for a detailed analysis of the process, is focused on the level shifts and widths [5] and on basic matrix elements [6], which are obtained by perturbative methods or by the coupled angular mode method [7]. The nonperturbative complex scaling method [8] has been used for calculating the same quantities for the hydrogenic Rydberg states. The one-electron exchanges investigated within the framework of the proposed schemes are mainly based on resonant (isoenergetic) models of the electron capture and ionization, which are considered as independent processes.

Recently, we analyzed [9,10] some beam-foil experimental data [11–13] concerning the Rydberg-level population of multiply charged ionic projectiles ($Z=6, 7$, and 8) at intermediate velocities ($v \sim 1$ a.u.), not yet studied by the above cited theoretical models. We found that a nonresonant one-electron exchange mechanism of the population reionization type is efficient when the ions escape a solid surface. A two-state formalism [9,10,14] of the Demkov-Ostrovskii type [15] has been adapted to the ion-surface problem.

Because of the complexity of the process, the problem has been treated within the fast-ionization approximation [10]. However, while using the proposed approximation we obtained an unphysical consequence: the ion-surface distances R_c^N and R_c^I , where the neutralization and reionization processes are mainly localized turned out to be equal. Also, in

the fast-ionization approximation, the reionization effect completely canceled the population probabilities P_{nl} for $n > n_{thr}$, where n_{thr} is the threshold value of the principal quantum number. As a result, some theoretical values for $n < n_{thr}$ have overestimated the experimental data (Figs. 5, 6, and 7 in Ref. [10]).

This paper is devoted to a systematic analysis of the reionization mechanism beyond the fast-ionization approximation. A phenomenological model based on the Hamiltonian $\hat{H}_2(t)$ is set up. The Hamiltonian $\hat{H}_2(t)$ is constructed by replacing the final-channel Hamiltonian $\hat{H}_2(t)$, within a finite “time window,” with the initial-channel Hamiltonian $\hat{H}_1(t)$. Thereby, a back transfer of active electrons from the moving ion into the solid, i.e., the reionization of previously populated Rydberg states, can be effected.

We calculate the reionization rate $\Gamma^I(t)$ in an analytic form by means of the complex parabolic eigenenergies of the Hamiltonian $\hat{H}_2(t)$. To do this we use the étalon equation method [16,17], adapted for deep under-barrier transitions as well as transitions in the vicinity of the potential barrier top. We point out that the dynamics of turning point configurations during the ionic motion plays an important role in the eigenvalue calculations; for different values of the ion-surface distances R , the configurations of relevant turning points can be very different.

The following physical picture of Rydberg-state reionization under the mentioned beam-foil experimental conditions emerges. First of all, the reionization process is strictly localized around some ion-surface distances R_c^I and the reionization rates have very pronounced single-peak forms at these distances. Second, the reionization of the Rydberg states $n > n_{thr}$ is delayed in comparison to the time $t_c^N = R_c^N/v$ when electron capture is dominant, so that these Rydberg states are characterized by very short but finite lifetimes. Finally, the reionization effect contributes not only to the region $n > n_{thr}$, but also to the curves of the overall “renormalized” population \bar{P}_{nl} , obtained under multichan-

*Electronic address: hekata@ff.bg.ac.yu

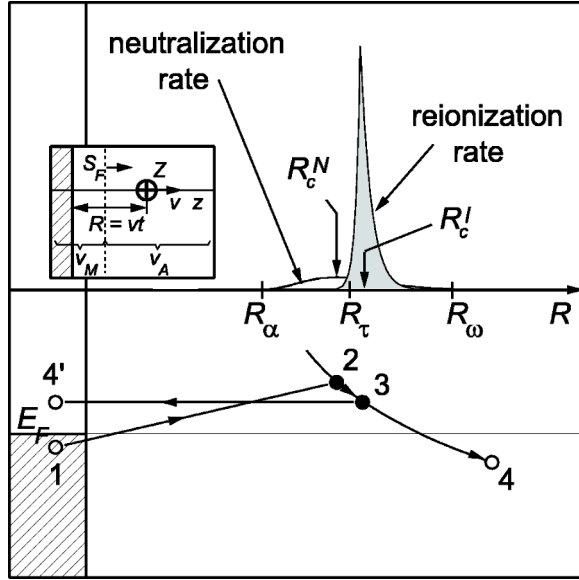


FIG. 1. The structure of the population-reionization process at intermediate velocities ($v \sim 1$) of the multiply charged ionic projectiles ($Z \gg 1$) at solid surfaces with Fermi level E_F .

nel conditions of the ion-surface interaction.

This paper is organized as follows. In Sec. II we formulate the problem by exposing the structure of the population-reionization process. Section III is devoted to an explicit study of the reionization mechanism. The calculations related to the reionization rate $\Gamma^I(t)$ are presented in Secs. III A, III B, and III C, whereas the probabilities \bar{P}_{nl} are calculated and compared with the available beam-foil data [11–13] in Sec. III D. Some concluding remarks will be given in Sec. IV.

Atomic units ($e^2 = \hbar = m_e = 1$) will be used throughout the paper unless indicated otherwise.

II. FORMULATION OF THE PROBLEM

A. Structure of the population-reionization process

We consider an electron exchange process in the ion-surface system (Fig. 1), supposing that the pointlike ionic projectile Z leaves the solid surface at $t_{in}=0$ and moves along the z axis according to the classical law $R=vt$. Roughly speaking, the population-reionization process, presented in Fig. 1, dominates during a time interval (t_α, t_ω) around the time $\tau \in (t_\alpha, t_\omega)$ when destruction of the intermediate Rydberg states begins. The quantities t_α and t_ω are auxiliary parameters introduced only to point out the localization of the process and they are absent from our final physically relevant expressions (see Sec. II C). The definition of the time τ is given in Sec. III C.

Initially, the active electron is predominantly localized inside a semi-infinite solid, with the work function ϕ and depth U_0 of the potential well of Sommerfeld's model (point 1 of the graph in Fig. 1). Nonresonant electron capture, described by the graph element 1 \rightarrow 2 in Fig. 1, occurs around large ion-surface distances $R \approx R_c^N$ and results in an intermediate Rydberg-state population (2 \rightarrow 3). Note that the points 2 and 3 would coincide exclusively within the framework of

the fast-ionization approximation [10]. Around the branching point 3 of the graph, corresponding to $R \approx R_c^I$, the active electron can be captured into the solid (3 \rightarrow 4'), but the intermediate Rydberg structure can also survive as a moving bound state mainly localized around the ionic projectile (3 \rightarrow 4).

If the electron exchange process ends at point 4 of Fig. 1, the photon deexcitation of the Rydberg state formed is registered by a detector in the beam-foil experimental setup [11–13], and we denote this final state the observable Rydberg state. However, if process finishes at point 4' there is no photon emission. In this case, the intermediate short-lived Rydberg state is unobservable for the detection system. The neutralization and reionization rates of the short-lived Rydberg states, also sketched in Fig. 1, partly overlap, which means that the electron capture is in competition with the reionization (around $R=R_\tau$). Note also that the proposed loop-type population-reionization process is not possible within the framework of resonant electron exchange models.

B. The initial- and final-channel Hamiltonians $\hat{H}_1(t)$ and $\hat{H}_2(t)$, and $\hat{H}_2(t)$

In order to describe the population process we define the initial- and final-channel Hamiltonians $\hat{H}_1(t)$ and $\hat{H}_2(t)$. The reionization model is embodied in the Hamiltonian $\hat{H}_2(t)$.

Initially, the active electron is almost completely localized inside the semi-infinite solid, so that [9,10] we can take $\hat{H}_1(t_{in}) = -\frac{1}{2}\nabla^2 + U_{1,in}$. The Sommerfeld potential well $U_{1,in}$ for $z < 0$ allows infinite electron motion along the negative part of the z axis. The final state is defined by the set of operators $\hat{H}_2(t_{fin})$, \hat{L}_z , and \hat{L}^2 , corresponding to the measurements [11–13] at the final time $t_{fin} \rightarrow \infty$. For sufficiently large ion-surface distances, the final state of the active electron is mainly localized around the ionic core and we have $\hat{H}_2(t_{fin}) = -\frac{1}{2}\nabla^2 + U_{2,fin}$, where $U_{2,fin}$ represents the Coulomb interaction for $z > 0$, whereas for $z < 0$ we take $U_{2,fin} = 0$.

The initial and final Hamiltonians $\hat{H}_1(t_{in})$ and $\hat{H}_2(t_{fin})$ can be “symmetrically” extrapolated to the initial- and final-channel Hamiltonians $\hat{H}_1(t)$ and $\hat{H}_2(t)$; namely, the Hamiltonian $\hat{H}_1(t)$ is defined by

$$\hat{H}_1(t) = -\frac{1}{2}\nabla^2 + U_1(t), \quad (2.1a)$$

where

$$U_1(t) = -U_0\Theta(-z) + [U_M + (U_A + U_{AM})]\Theta(z), \quad (2.1b)$$

where $\Theta(z)$ represents the Heaviside function. We denoted by U_A , U_M , and U_{AM} the Coulomb potential and the potentials of the electron interactions with the proper image and the core image, respectively.

The final-channel Hamiltonian $\hat{H}_2(t)$ is defined by

$$\hat{H}_2(t) = -\frac{1}{2}\nabla^2 + U_2(t), \quad (2.2a)$$

where

$$U_2(t) = [U_A + (U_M + U_{AM})]\Theta(z). \quad (2.2b)$$

Note that $U_1 \rightarrow U_{1,in}$ for $t \rightarrow t_{in}$ and $U_2 \rightarrow U_{2,fin}$ for $t \rightarrow t_{fin}$.

For $R \gg 1$, the potentials $U_A + U_{AM}$ and $U_M + U_{AM}$ [Eqs. (2.1b) and (2.2b)], can be replaced by the corresponding asymptotic expressions, so that parabolic and spherical representations of the eigenfunctions of the Hamiltonians $\hat{H}_1(t)$ and $\hat{H}_2(t)$, respectively, are possible. Note that in a wide region around the ionic core a parabolic representation of the $\hat{H}_2(t)$ eigenfunctions is also possible.

The Hamiltonian $\hat{H}_2(t)$ is defined by the following expression:

$$\hat{H}_2(t) = \begin{cases} \hat{H}_2(t), & t \in [t_\alpha, t_\omega], \\ \hat{H}_1(t), & t \in [t_\alpha, t_\omega]. \end{cases} \quad (2.3)$$

The proposed Hamiltonian $\hat{H}_2(t)$ will also be considered in the asymptotic region ($R = vt \gg 1$), where a parabolic representation of its eigenfunctions is possible. Because of the outgoing wave boundary condition in the solid, imposed on the eigenfunctions, the corresponding eigenenergies are complex quantities.

C. The wave function $\bar{\Psi}_2(\vec{r}, t)$

In the two-state model [10], the population process is described by the probability amplitude $A(t) = \langle \Psi_2(t) | \hat{P}_A(t) | \Psi_1(t) \rangle$, where $\hat{P}_A = \Theta(z - z_F)$, whereas z_F is the instant position of the Firsov plane S_F (see Fig. 1). In the vicinity of the S_F plane we have [9,10], $|\Psi_1(t)\rangle = \exp(\hat{h}_M) |\Phi_{MA, \mu_{M,in}}^{(1)}\rangle$ and $|\Psi_2(t)\rangle = \exp(\hat{h}_A) |\Phi_{AM, \nu_{A,fin}}^{(2)}\rangle$, where \hat{h}_M and \hat{h}_A contribute to small corrections of the parabolic eigenstates $|\Phi_{MA, \mu_{M,in}}^{(1)}\rangle$ and spherical eigenstates $|\Phi_{AM, \nu_{A,fin}}^{(2)}\rangle$ of the Hamiltonians $\hat{H}_1(t)$ and $\hat{H}_2(t)$.

The population-reionization process is described by the probability amplitude $\bar{A}(t) = \langle \bar{\Psi}_2(t) | \hat{P}_A(t) | \Psi_1(t) \rangle$, where

$$|\bar{\Psi}_2(t)\rangle = \Theta(\tau - t) |\Psi_2(t)\rangle + \Theta(t - \tau) \hat{U}_2(\tau, t) |\Psi_2(\tau)\rangle, \quad (2.4)$$

whereas $\hat{U}_2(\tau, t)$ is the evolution operator determined by the Hamiltonian $\hat{H}_2(t)$. In writing Eq. (2.4) we assumed that the effect of the reionization in the time interval $[t_\alpha, \tau]$ could be neglected; namely, for the short-lived Rydberg states the reionization rate is negligible for $t < \tau$, and for the long-lived Rydberg states (where the positions of the maxima of reionization and neutralization rates are inverted in comparison to the short-lived ones) the neutralization rate is negligible for $t < \tau$. Note that the state $|\bar{\Psi}_2(t)\rangle$ expressed by Eq. (2.4) is independent of t_α .

A procedure based on the spectral decomposition of the Hamiltonian $\hat{H}_2(t)$ (which we shall present in detail elsewhere) will give an explicit form of Eq. (2.4). Here we use an asymptotic form of Eq. (2.4), describing the decaying state $|\bar{\Psi}_2(t)\rangle$ during the population-reionization process. The state $|\bar{\Psi}_2(t)\rangle$ is represented by the superposition

$$\begin{aligned} |\bar{\Psi}_2(t)\rangle &= \Theta(\hat{z}) \sum_{\mu_A} \langle \Phi_{AM, \mu_A}^{(2)} | \Psi_2(t) \rangle \\ &\times \exp\left(-\frac{1}{2}\Theta(t - \tau) \int_\tau^{t_{min}} \Gamma_{\mu_A}^I dt\right) |\Phi_{AM, \mu_A}^{(2)}\rangle \\ &+ \Theta(t - \tau) \Theta(-\hat{z}) |\chi(t)\rangle, \end{aligned} \quad (2.5)$$

where $|\Phi_{AM, \mu_A}^{(2)}\rangle$ are the parabolic eigenstates of the Hamiltonian $\hat{H}_2(t)$, $\Gamma_{\mu_A}^I$ is the reionization rate from the parabolic intermediate state $\mu_A = (n_A, n_{1A}, m_A)$, and $|\chi(t)\rangle$ is the electron state (outgoing wave) inside the solid. The upper limit of integration in Eq. (2.5) is given by $t_{min} = \min(t, t_\omega)$.

By means of Eq. (2.5), we express the amplitude $\bar{A}(t)$ as a sum over μ_A . Using the approximate expressions for $|\Psi_1(t)\rangle$ and $|\Psi_2(t)\rangle$, valid on the Firsov plane, we can specify a set of intermediate parabolic quantum numbers μ_A which give the main contribution to the probability amplitude. We get

$$\mu_{A0} = (n_A = n(1 + \mathcal{O}), \quad n_{1A} = \mathcal{O}, \quad m_A = 0), \quad (2.6)$$

where $\mathcal{O} = \mathcal{O}(1/R)$; namely, the active electron is mainly captured from the parabolic initial state $\mu_{M,in} = (\gamma, n_{1M} = 0, m_M = 0)$ (Ref. [10]), via an intermediate parabolic state with $\mu_A = (n_A \approx n, n_{1A} \approx 0, m_A = 0)$ into the final spherical state $\nu_{A,fin} = (n, l, m = 0)$.

Therefore, the wave function $\bar{\Psi}_2(\vec{r}, t) = \langle \vec{r} | \bar{\Psi}_2(t) \rangle$ can be expressed as

$$\bar{\Psi}_2(\vec{r}, t) = \Theta(z) \mathcal{E}_{\mu_{A0}}(t) \Psi_2(\vec{r}, t) + \Theta(-z) \chi(\vec{r}, t), \quad (2.7)$$

where

$$\mathcal{E}_{\mu_{A0}}(t) = \exp\left(-\frac{1}{2}\Theta(t - \tau) \int_\tau^{t_{min}} \Gamma_{\mu_{A0}}^I(t) dt\right). \quad (2.8)$$

Note that the factor $\mathcal{E}_{\mu_{A0}}(t)$ changes the norm of the wave function $\bar{\Psi}_2(\vec{r}, t)$ for $z > 0$, i.e., the state Ψ_2 is renormalized. The reionization rate $\Gamma_{\mu_{A0}}^I$ is given by

$$\Gamma_{\mu_{A0}}^I = -2\text{Im}E_{A, \mu_{A0}}^{(1)}(R), \quad (2.9)$$

where $E_{A, \mu_{A0}}^{(1)}(R)$ are the complex eigenenergies of the Hamiltonian $\hat{H}_2(t) = \hat{H}_1(t)$ in the time interval $[t_\alpha, t_\omega]$ [Eq. (2.3)]. Taking into account that $\Gamma_{\mu_{A0}}^I \approx 0$ for $t > t_\omega$, the upper limit t_{min} of integration in Eq. (2.8) can be replaced by t . Thereby, the time t_ω is absent in our subsequent calculations.

Although the expression (2.9) resembles the conventional decay rate, we point out that its origin is in the two-state formalism; namely, the rate $\Gamma_{\mu_{A0}}^I$ incorporates relevant information from both the initial and final electron states (the points 1 and 4 \cup 4' in Fig. 1) through the set μ_{A0} . Note also that the decay factor $\mathcal{E}_{\mu_{A0}}(t)$ depends on the ionic velocity v , via the ionic motion law ($R=vt$) and on lower limit $\tau = \tau(v)$ of integration [Eq. (2.8)].

III. THE REIONIZATION MECHANISM

A. The reionization rate $\Gamma^I(t)$

In our previous study [10] of the Rydberg-level population-reionization process, we estimated the reionization factor $\mathcal{E}_{\mu_{A0}}(t)$ by setting $\mathcal{E}_{\mu_{A0}}(\infty)=0$ beyond the threshold values of n . Here we expose relevant facts for obtaining an asymptotically accurate analytic expression for the reionization rate $\Gamma_{\mu_{A0}}^I(t)$ yielding a nonvanishing value of $\mathcal{E}_{\mu_{A0}}(t)$ for $n > n_{thr}$. The reionization rate $\Gamma_{\mu_{A0}}^I(t)$ is given by Eq. (2.9) in terms of the complex eigenenergies $\bar{E}=E_{A,\mu_{A0}}^{(1)}(R)$. Accordingly, within the proposed approximations, the problem of the $\Gamma_{\mu_{A0}}^I(t)$ evaluation is reduced to an eigenvalue problem of the Hamiltonian $\hat{H}_2(t)=\hat{H}_1(t)$ around $t=\tau$.

In the asymptotic region ($R \gg 1$), for $n \gg 1$ and $Z \gg 1$, the eigenvalue problem of the Hamiltonian $\hat{H}_1(t)$ can be solved in the analogous manner as in Ref. [10], but under the outgoing wave condition inside the solid. We use the scaled parabolic coordinates $\tilde{\xi}$, $\tilde{\eta}$, and φ with the complex scaling parameter $\bar{\alpha} = -2\bar{E}R/(Z-1/4)$, and apply the étalon equation method [16,17]. For $\alpha = \text{Re}\bar{\alpha} \sim \alpha_0$ we have a configuration of the close turning points $\tilde{\eta}_1$ and $\tilde{\eta}_2$ [10]. The distance between the turning points increases with increase of α so that the condition $\alpha \gg \alpha_0$ describes the distant turning point configuration. The quantity $\alpha_0 \sim 1$, representing the scaling parameter for the confluent turning points ($\tilde{\eta}_1 \approx \tilde{\eta}_2$), is determined uniquely [10] by the ionic core charge Z .

As a result, we obtain the following expression for the real part of the energy $E_{A,\mu_A}^{(1)}(R)$:

$$\text{Re}E_{A,\mu_A}^{(1)} = -\frac{Z^2}{2n_A^2} + \frac{2Z-1}{4R} - \frac{3}{8} \frac{Z-1}{Z} \frac{n_A}{R^2} (n_{1A} - n_{2A}) + \dots, \quad (3.1a)$$

where n_{2A} is the second parabolic quantum number ($n_{1A} + n_{2A} + |m_A| + 1 = n_A$). The reionization rate $\Gamma_{\mu_A}^I = -2\text{Im}E_{A,\mu_A}^{(1)}$ [Eq. (2.9)] is given by

$$\Gamma_{\mu_A}^I(t) = \frac{Z^2}{\pi n_A^3} D(\lambda, \alpha), \quad (3.1b)$$

where $D(\lambda, \alpha) = \min(D_1(\lambda, \alpha), D_0(\lambda, \alpha))$, and

$$D_1(\lambda, \alpha) = \left(\frac{e^{3\alpha-2}}{4\alpha} \right)^{2\lambda} D_0(\lambda, \alpha). \quad (3.2)$$

For the function $D_0(\lambda, \alpha)$ we have

$$D_0(\lambda, \alpha) = \left(\frac{bp_0e}{\lambda} \right)^{2\lambda} \exp(-bF + 2\lambda p_0G), \quad (3.3)$$

where $\lambda = n_{2A} + (|m_A| + 1)/2$ and $b = 2R\alpha(-2\text{Re}E_{A,\mu_A}^{(1)})^{1/2}$. The functions F and G are determined by

$$F = \frac{p_0}{\alpha} \left(1 - \frac{3}{2C_0} \frac{1}{2\alpha} \right) + \frac{C_1}{2\alpha p_1} \ln \left(\frac{p_1 - p_0}{p_1 + p_0} \right) + \frac{C_2}{2\alpha\sqrt{C_0}} \left(1 - \frac{C_1}{C_2} + \frac{3}{4\alpha C_0} \right) \ln \left(\frac{\sqrt{C_0} - p_0}{\sqrt{C_0} + p_0} \right), \quad (3.4a)$$

$$G = \frac{1}{\sqrt{C_0}} \ln \left(\frac{\sqrt{C_0} - p_0}{\sqrt{C_0} + p_0} \right) + \frac{1}{p_0} \ln \left(\frac{4p_0^2}{C_2\alpha} \right). \quad (3.4b)$$

The quantities C_i , $i=0, 1$, and 2 , are defined by $C_0 = 1 + 3/(2\alpha)$, $C_1 = 2(2-Z_0)/\alpha$, and $C_2 = 2(1-Z_0)/\alpha$, whereas $p_0 = (C_0 - C_2)^{1/2}$ and $p_1 = (C_0 + C_2)^{1/2}$. Note that the Z dependences in the functions F and G are exclusively localized in the quantity $Z_0 = (Z-1/2)/(Z-1/4)$. For $Z \gg 1$, the Z dependences are very weak, so that F and G can be considered as universal functions of α .

The result (3.1a) can be interpreted as the energy of a hydrogenlike atom in an effective homogeneous electric field $\tilde{F} = (1-Z)/(4R^2)$ (obtained by the first-order perturbative method), shifted by the term $\Delta E = (2Z-1)/(4R)$. In the two-state model, the specific character of Eq. (3.1a) is manifested only through the choice of the active member of the energy manifold [$\mu_A = \mu_{A0}$; Eq. (2.6)]. However, the result (3.1b) differs significantly from the ionization rates obtained within the framework of the previous asymptotic one-state models [18,19]. The first difference appears due to the factor $D(\lambda, \alpha)$, which takes into account the specificity of the turning point configuration. The second difference is in determining the rate $\Gamma_{\mu_{A0}}^I(t)$ by imposing both initial and final conditions.

B. R and α dependences of the reionization rate

In order to obtain the reionization rate $\Gamma_{\mu_{A0}}^I$ as a function of R , we note that the real part α of the scaling parameter $\bar{\alpha}$ depends not only explicitly on R , but also implicitly via the energy given by Eq. (3.1a). Accordingly, in the first approximation, we can take $\alpha(R) = [Z^2/n^2 - (2Z-1)/(2R)]R/(Z-1/4)$.

In Fig. 2 we present the R dependence of the rate $\Gamma_{\mu_{A0}}^I = \Gamma_{\mu_{A0}}^I(t)$ for the short-lived Rydberg states of the Cl VII ion with $10 \leq n \leq 14$. The Γ^I curves have very pronounced peaks at the critical ion-surface distances estimated by $R = R_c^I \sim 2n^2/Z$. The reionization rates of the observable Rydberg states ($n < 10$) are significantly smaller in comparison to the presented ones.

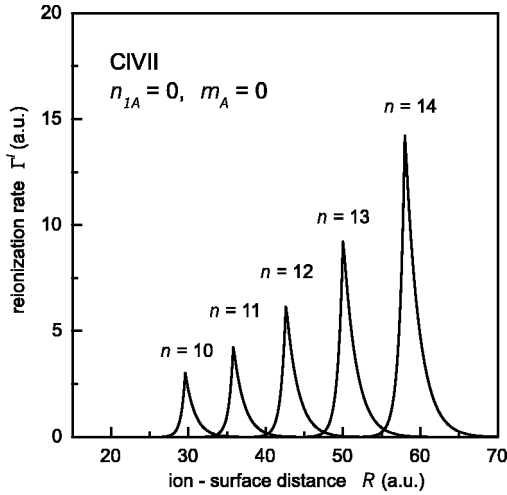


FIG. 2. The reionization rate $\Gamma^I = \Gamma_{\mu_{A0}}^I(t)$ of the Cl VII ion for the short-lived Rydberg states $\mu_{A0} = (n_A = n \geq 10, n_{1A} = 0, m_A = 0)$ presented as a function of the ion-surface distance R .

A comparison of the $R = R_c^I$ values with the positions $R = R_c^N$ of the neutralization maxima obtained on the basis of Eq. (4.9) from Ref. [10] leads us to a nontrivial conclusion about the mutual positions of the Γ^N and Γ^I maxima on the R axis; namely, for all considered values of the quantum number n , each Γ^N maximum is followed by a Γ^I maximum. In Table I we present the quantities R_c^N and R_c^I for a Cl VII ion escaping from the solid surface with the velocity $v = 2.50$. We consider the short-lived states with $v_{A,fin} = (n, l = 1, m = 0)$ for $n > n_{thr} = 9$. Also, we take $\mu_{M,in} = (\gamma_{in}, n_{1M,in} = 0, m_{M,in} = 0)$, where $\gamma_{in} = \gamma_F = 0.47$ for $n > 10$ and $\gamma_{in} = 0.50$ for $n = 10$. Similar numerical results can be presented for short-lived Rydberg states of the ions S VI and Ar VIII.

Note that the critical distances $R_c^I \sim n^2/Z$ obtained within the framework of the asymptotic JWKB approach [19] are about one-half the value of R_c^I from Fig. 2. It is also worth noting that the energy widths obtained by the perturbation method [5] exhibit a series of oscillations along the R axis. The most distant maximum of these oscillations is localized at $R_c^I \sim 2n^2/Z$, i.e., at the position of the strongly localized reionization rate Γ^I . The absence of oscillations from the reionization rates for $R < R_c^I$ can be explained by the following fact: the reionization process can be activated after the neutralization process has been mainly realized. Also, the greatest magnitude of the rate obtained by the nonperturbative coupled angular mode method [20] is positioned approximately at the same point (for $n_1 = 0, n_2 = n - 1, m = 0$).

TABLE I. Critical distances of the population-reionization process for the Cl VII ion escaping the solid surface with $v = 2.50$.

n	10	11	12	13	14
R_c^N	28.2	32.5	37.8	43.2	48.9
R_c^I	29.6	35.9	42.6	50.0	58.0

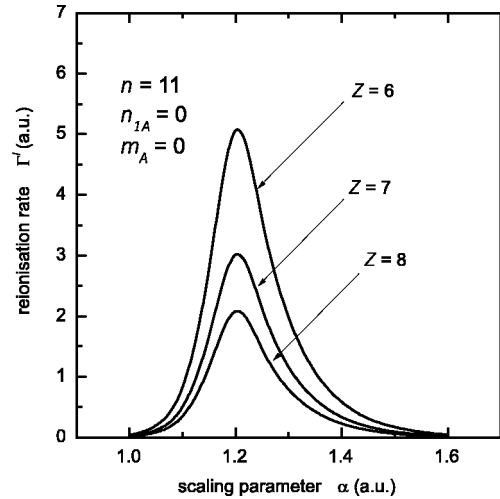


FIG. 3. The reionization rate $\Gamma^I = \Gamma_{\mu_{A0}}^I(t)$ of the Cl VII ion for the short-lived Rydberg states $\mu_{A0} = (n_A = n = 11, n_{1A} = 0, m_A = 0)$ presented as a function of the scaling parameter α .

Universality of the reionization process can be deduced from the α dependence of the rate $\Gamma_{\mu_{A0}}^I$. The relevant graphs are presented in Fig. 3, for the Rydberg states $n_A = n = 11$ of the ions S VI, Cl VII, and Ar VIII. The $\Gamma_{\mu_{A0}}^I$ curves have very pronounced peaks for the same critical value of the scaling parameter α . We obtain the same universality for all principal quantum numbers n .

The positions of the presented maxima, $\alpha \approx \alpha_0 \sim 1$, indicate that the reionization of the state considered is in the vicinity of the potential barrier top. This quantum prediction correlates with the general assumption of the classical over-barrier model [1].

C. The renormalized neutralization rate

By including the reionization effect in the Rydberg-state population process, at intermediate stages of the ion-surface interaction, we obtain the renormalized transition probability $\bar{T}_{v_{A,fin}}^{N,\mu_{M,in}}(t)$. For a given initial state $\mu_{M,in}$ we get $\bar{T}_{v_{A,fin}}^{N,\mu_{M,in}}(t) = \mathcal{E}_{\mu_{A0}}(t) T_{v_{A,fin}}^{N,\mu_{M,in}}(t)$, i.e.,

$$\bar{T}_{v_{A,fin}}^{N,\mu_{M,in}}(t) = \exp\left(-\Theta(t-\tau) \int_{\tau}^t \Gamma_{\mu_{A0}}^I(t) dt\right) \times \left[1 - \exp\left(-\int_{t_{in}}^t \Gamma_{v_{A,fin}}^{N,\mu_{M,in}}(t) dt\right)\right], \quad (3.5)$$

where $\Gamma_{v_{A,fin}}^{N,\mu_{M,in}}(t)$ is the neutralization rate [10]. The corresponding renormalized neutralization rate is given by $\bar{\Gamma}_{v_{A,fin}}^{N,\mu_{M,in}}(t) = d\bar{T}_{v_{A,fin}}^{N,\mu_{M,in}}(t)/dt$. The parameter τ is defined by the condition $\bar{\Gamma}^N(\tau) = 0$.

In the case of short-lived Rydberg states the neutralization and reionization processes are mainly localized within time intervals $t \in [t_{\alpha}, \tau]$ and $t \in [\tau, t_{\omega}]$, respectively; for example, see Fig. 1. Therefore, taking into account that $\Gamma_{\mu_{A0}}^I(\tau) \approx \Gamma_{v_{A,fin}}^{N,\mu_{M,in}}(\tau)/T_{v_{A,fin}}^{N,\mu_{M,in}}(\infty)$, we get

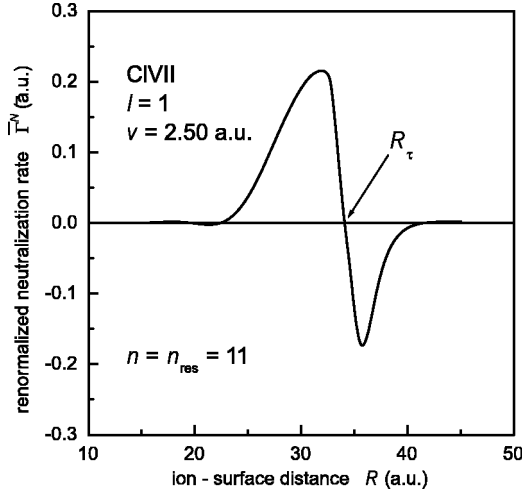


FIG. 4. The renormalized neutralization rate $\bar{\Gamma}^N = \bar{\Gamma}_{\nu_{A,fin}}^{N, \mu_{M, in}}(t)$ per unit γ_{in} for the Cl VII ion escaping the solid surface with $v = 2.50$; $\mu_{M, in} = (\gamma = \gamma_F, n_{1M} = 0, m_{M, in} = 0)$ and $\nu_{A, fin} = (n = 11, l = 1, m = 0)$.

$$\bar{\Gamma}_{\nu_{A, fin}}^{N, \mu_{M, in}}(t) = \mathcal{E}_{\mu_{A0}}^2(\infty) [\Gamma_{\nu_{A, fin}}^{N, \mu_{M, in}}(t) - \Gamma_{\mu_{A0}}^I(t) T_{\nu_{A, fin}}^{N, \mu_{M, in}}(\infty)], \quad t > \tau, \quad (3.6)$$

and $\bar{\Gamma}_{\nu_{A, fin}}^{N, \mu_{M, in}}(t) = \Gamma_{\nu_{A, fin}}^{N, \mu_{M, in}}(t)$ for $t < \tau$. In order to evaluate the quantity $\mathcal{E}_{\mu_{A0}}^2(\infty)$ appearing in Eq. (3.6), it is convenient to replace the integration over the time $t \in [\tau, t_\omega]$ in Eq. (2.8) by an integration over the scaling parameter $\alpha \in [\alpha_\tau, \infty]$, where $\alpha_\tau = \alpha(R_\tau)$. Accordingly, the quantity $\mathcal{E}_{\mu_{A0}}^2(\infty)$ can be expressed as follows:

$$\mathcal{E}_{\mu_{A0}}^2(\infty) = \exp \left[-\frac{n^2}{vZ} \left(1 - \frac{1}{4Z} \right) \int_{\alpha_\tau}^{\infty} \Gamma_{\mu_{A0}}^I d\alpha \right]. \quad (3.7)$$

By performing the numerical calculations based on Eqs. (3.6) and (3.7) we obtain the rate $\bar{\Gamma}_{\nu_{A, fin}}^{N, \mu_{M, in}}(t)$ for all relevant values of the ion-surface parameters.

As an example of the rate $\bar{\Gamma}^N(t)$, we consider again the Cl VII ion with the velocity $v = 2.50$. We present the physically most important case $n = n_{res} = 11$, $l = 1$, $m = 0$ corresponding to the (unobservable) resonant Rydberg level $n = n_{res}$. For the energy parameter γ we take the value γ_F corresponding to the Fermi level of the solid ($\phi = 3$ eV). The relevant quantum numbers of the intermediate parabolic state, Eq. (2.7), are determined by the set $\mu_{A0} = (n_A = n = 11, n_{1A} = 0, m_A = 0)$. In that case we have $T_{\nu_{A, fin}}^{N, \mu_{M, in}}(\infty) = 1.17$ and $R_\tau = v\tau = 34.01$, whereas $\mathcal{E}_{\mu_{A0}}^2(\infty) = 5.1 \times 10^{-2}$.

In Fig. 4 we present the R dependence of the rate $\bar{\Gamma}^N = \bar{\Gamma}_{\nu_{A, fin}}^{N, \mu_{M, in}}(t)$ for the Cl VII ion, with the cited numerical values of the relevant parameters. We note that the presented $\bar{\Gamma}^N$ curve does not represent a simple ‘‘superposition’’ of the neutralization and reionization rates Γ^N and Γ^I ; compare, for

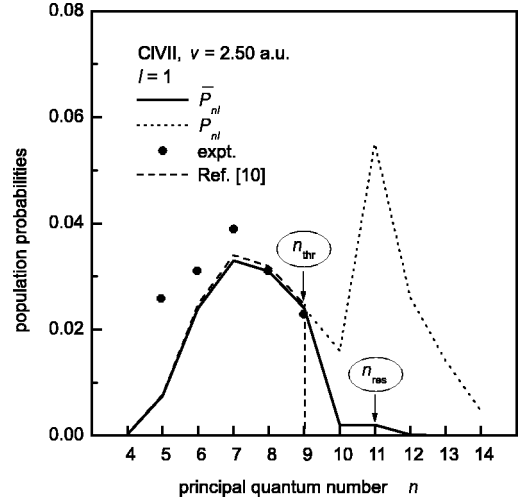


FIG. 5. Effect of the reionization in the $n > n_{thr}$ region for the Cl VII ion with $l = 1$ and $v = 2.50$. Dots are experimental data taken from Ref. [12]. The dashed curve is obtained under the fast-ionization assumption (Ref. [10]).

example, the maximal value of Γ^I for $n = 11$ in Fig. 2 with the minimal value of $\bar{\Gamma}^N$ in Fig. 4.

D. The renormalized population probability \bar{P}_{nl} and comparison with experiments

The results obtained in Sec. III C can be used in our final calculations of the experimentally verifiable probability \bar{P}_{nl} . Due to the multichannel character of the process [10], the existence of the short-lived Rydberg states is manifested through the thresholdlike forms of the population curves, as well as their overall forms. Accordingly, the \bar{P}_{nl} curves can be significantly different in comparison to the nonrenormalized population curves P_{nl} .

For time $t = t_{fin} = \infty$ the probabilities \bar{P}_{nl} and P_{nl} are related by

$$\bar{P}_{nl} = [\Theta(\tau - t_F) + \Theta(t_F - \tau) \mathcal{E}_{\mu_{A0}}^2(\infty)] P_{nl}, \quad (3.8)$$

where $t_F = R_F/v$, whereas the distance R_F is determined by $\text{Re}E_{A, \mu_{A0}}^{(1)}(R_F) = -\phi$. From the expression (3.8) we conclude that, for $t_F > \tau$, the physically relevant population probability \bar{P}_{nl} differs from the nonrenormalized probability P_{nl} by the factor $\mathcal{E}_{\mu_{A0}}^2(\infty)$, which can be calculated by means of Eq. (3.7).

Among the various possible presentations of probability \bar{P}_{nl} we will show those curves that reflect three characteristic consequences of the reionization effect.

In Fig. 5 we present the \bar{P}_{nl} curve for the case of Cl VII ion with $l = 1$ and $v = 2.50$. In the same figure we also present the nonrenormalized curve P_{nl} , with all channels opened, obtained by the method from Ref. [10]. The dashed curve is the population probability [10], obtained under the fast-ionization condition (i.e., the channels $n > n_{thr}$ are closed). The experimental points are taken from Ref. [12].

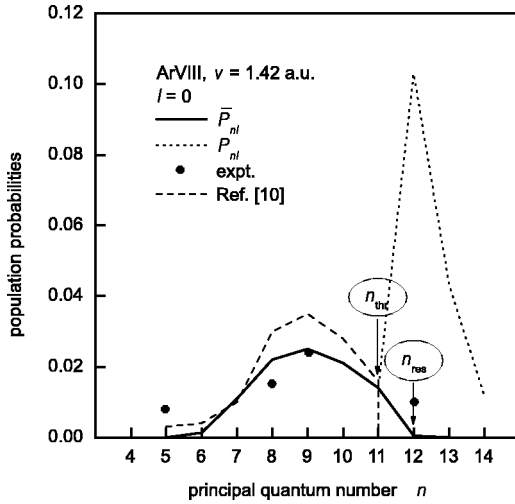


FIG. 6. Effects of the reionization in the $n > n_{thr}$ and $n < n_{thr}$ regions for the Ar VIII ion with $l=0$ and $v=1.42$. Dots are experimental data taken from Ref. [12]. The dashed curve is obtained under the fast-ionization assumption (Ref. [10]).

The reionization effect is quite evident: the renormalized \bar{P}_{nl} peak at $n = n_{res} = 11$ is about 10 times smaller than the non-renormalized one. Under real experimental conditions, the local \bar{P}_{nl} peak at $n = 11$ essentially represents an unobservable structure on the graph in comparison to the “visible” part around $n_0 \approx Z = 7$. A set of the \bar{P}_{nl} graphs, similar to the one presented, can also be obtained for $l=0$ and $l=2$ of the Cl VII ion, as well as for the S VI ion with $l=0, 1$, and 2 .

The \bar{P}_{nl} curve of the Ar VIII ion with $l=0$ and $v=1.42$ is presented in Fig. 6. The meaning of the additional two curves presented in Fig. 6 is the same as in Fig. 5. For the resonance level $n = n_{res} = 12$, we have $\tau < t_F$ (i.e., the element $2 \rightarrow 3$ of the graph in Fig. 1 is above the Fermi level E_F ; the same holds for the state $n = 11$ of the Cl VII ion in Fig. 5). Note that, in contrast to Fig. 5, the \bar{P}_{nl} curve and the dashed curve (obtained in Ref. [10]) under the fast-ionization condition) are different in the region $n < n_{thr}$.

In Fig. 7 we present the relevant population curves for the Ar VIII ion with $l=1$ and $v=1.42$. Note the change in scale: the probabilities \bar{P}_{nl} presented in Fig. 7 are about 10 times higher in comparison to those in Fig. 6. The existence of the pronounced \bar{P}_{nl} resonance shape at $n = n_{res} = 11$ is a consequence of the condition $\tau > t_F$. The reionization does not directly change the population of the resonance state ($n_{res} < n_{thr}$); the only modification of the population probability of the state $n = n_{res}$ is through the multichannel effect. (Compare the probability \bar{P}_{nl} with the probability P_{nl} taken from Ref. [10].) The same conclusion stands for the level $n = 11, l=2$ of the Ar VIII projectile with $v=1.42$.

IV. CONCLUDING REMARKS

The subject of this paper is the Rydberg-state reionization of multiply charged ions escaping solid surfaces at intermediate velocities, in the beam-foil interaction geometry. The

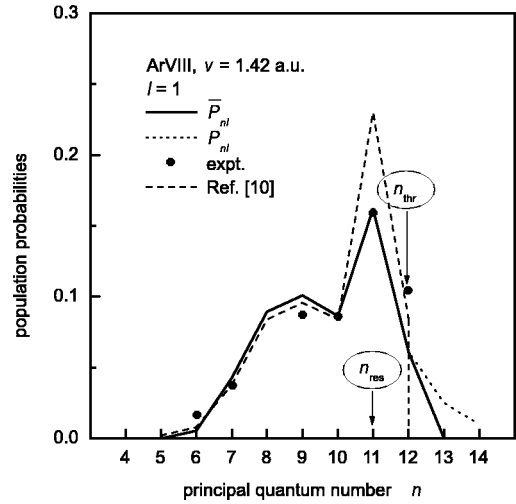


FIG. 7. Effect of the reionization in the $n \approx n_{res}$ region for the Ar VIII ion with $l=1$ and $v=1.42$. Dots are experimental data taken from Ref. [12]. The dashed curve is obtained under the fast-ionization assumption (Ref. [10]).

applied two-state formalism gives insight into both the intermediate and final stages of the population-reionization process. The calculated reionization rates take into account the vicinity of the potential barrier top. We found that the dynamics of the turning point configuration during the ionic motion, combined with the condition (2.6), results in single-peak forms of the R -dependent rates $\Gamma_{\mu A 0}^I$. The renormalized neutralization rate Γ^N is introduced in order to describe the influence of reionization on the electron capture process. The exposed model of the population-reionization process gives the population probabilities \bar{P}_{nl} , which represent nonlinear functions of the principal quantum number n , with one or two local maxima. Our explicit calculations are related to the case of low- l values of the Rydberg states (e.g., $l=0, 1$, and 2), with the projectile velocities v taken from experiments.

A few additional remarks may be relevant for subsequent investigation of the subject discussed in the paper.

First, the beam-foil experimental data [11–13] report a set of nonlinear l distributions characterized by threshold values $l_{thr} < n - 1$ in the large- l region. In this region we found that the reionization effect becomes important. The high- l population probability obtained within the framework of the two-state model [21] correlates with available experimental facts for S VI, Cl VII, and Ar VIII ions.

Second, it is possible to study the velocity dependence of the theoretical $\bar{P}_{nl}(v)$ curves and compare the results with the beam-foil experimental data reported in Ref. [22]. Most of the v data in the cited paper concern the high- l Rydberg states of multiply charged projectiles, so that the reionization effect can be very significant for an explanation of the experiment. In that sense, the results previously obtained [9] for the v dependences of the low- l population curves can be completed by the large- l curves.

Third, the population-reionization model can also be extended to the cases where ionic core projectiles cannot be regarded as pointlike charges; namely, the reported popula-

tion curves [23] for the ions Kr VIII and Xe VIII transferred through the same carbon foils, at practically the same intermediate velocities, are very different. We realized that this fact could be attributed to a screening effect, described by the Simons-Bloch type [24] of ionic core potential.

Finally, taking into account that the beam-foil experiments [11–13] were not designed for direct observation of the reionization, additional experimental work would be necessary for establishing the R_c^I values. Up to now, only a few experiments (see, for example, Refs. [25], [26], and [27]) have been devoted to direct measurement of the ionization distance R_c^I , but the data are associated with neutral Rydberg atoms approaching the surface at low velocities. In spite of the fact that these experiments differ significantly from the

beam-foil experiments discussed here, a theoretical study of the low- v experiments is possible within the framework of the two-state model. For example, our preliminary calculations related to the experimental conditions described in Ref. [27] indicate that the confluence of the turning points in the étalon equation method leads to correct critical ion-surface distances R_c^I .

ACKNOWLEDGMENT

This work was supported in part by the Ministry of Development, Science and Technologies, Republic of Serbia (Project No. 1470).

-
- [1] J. Burgdörfer, in *Review of Fundamental Processes and Applications of Atoms and Molecules*, edited by C.D. Lin (World Scientific, Singapore, 1993).
- [2] J. Burgdörfer, P. Lerner, and F. Meyer, *Phys. Rev. A* **44**, 5674 (1991).
- [3] J. Ducrée, F. Casali, and U. Thumm, *Phys. Rev. A* **57**, 338 (1998).
- [4] J. Ducrée, H. J. Andrä, and U. Thumm, *Phys. Rev. A* **60**, 3029 (1999).
- [5] U. Wille, *Phys. Rev. B* **50**, 1888 (1994).
- [6] P. Kürpick and U. Thumm, *Phys. Rev. A* **54**, 1487 (1996).
- [7] A. Borisov, R. Zimny, D. Teillet-Billy, and J. Gauyacq, *Phys. Rev. A* **53**, 2457 (1996).
- [8] P. Nordlander, *Phys. Rev. B* **53**, 4125 (1996).
- [9] N. N. Nedeljković, Lj. D. Nedeljković, S. B. Vojvodić, and M. A. Mirković, *Phys. Rev. B* **49**, 5621 (1994).
- [10] Lj. D. Nedeljković and N. N. Nedeljković, *Phys. Rev. B* **58**, 16455 (1998).
- [11] B. Andreson, B. Denne, J. Ekberg, L. Engstrom, S. Huldt, I. Martinson, and E. Veje, *Phys. Rev. A* **23**, 479 (1981).
- [12] S. Bashkin, H. Oona, and E. Veje, *Phys. Rev. A* **25**, 417 (1982).
- [13] E. Veje and H. Winter, *Z. Phys. D: At., Mol. Clusters* **10**, 457 (1988).
- [14] N. N. Nedeljković, Lj. D. Nedeljković, R. K. Janev, and Z. L. Mišković, *Nucl. Instrum. Methods Phys. Res. B* **58**, 519 (1991).
- [15] Yu. N. Demkov and V. N. Ostrovskii, *Zh. Eksp. Teor. Fiz.* **69**, 1582 (1975).
- [16] S. Yu. Slavyanov, *Diff. Eq.* **5**, 313 (1969) (in Russian).
- [17] S. Yu. Slavyanov, in *Problems in Mathematical Physics*, edited by M. S. Birman (Leningrad State University, Leningrad, 1970), Vol. 4, p. 125 (in Russian).
- [18] A. V. Chaplik, *Zh. Eksp. Teor. Fiz.* **54**, 332 (1968).
- [19] N. N. Nedeljković, *Fizika (Zagreb)* **12**, 275 (1980).
- [20] A. G. Borisov and U. Wille, *Surf. Sci. Lett.* **338**, L875 (1995).
- [21] N. N. Nedeljković, Lj. D. Nedeljković, and M. A. Mirković (unpublished).
- [22] C. Jupen, B. Denne, J. O. Ekberg, L. Engstrom, U. Litzen, I. Martinson, W. Tai-Meng, A. Trigueiros, and E. Veje, *Phys. Rev. A* **26**, 2468 (1982).
- [23] R. Hallin, J. A. Leavitt, A. Lindgard, P. W. Rathmann, H. Vach, and E. Veje, *Nucl. Instrum. Methods Phys. Res.* **41**, 202 (1982).
- [24] G. Simons and A. N. Bloch, *Phys. Rev. B* **7**, 2754 (1973).
- [25] C. Fabre, M. Gross, J. Raimond, and S. Haroche, *J. Phys. B* **16**, L671 (1983).
- [26] C. Kocher and R. Taylor, *Phys. Lett.* **68A**, 124 (1987).
- [27] S. B. Hill, C. B. Haich, Z. Zhou, P. Nordlander, and F. B. Dunning, *Phys. Rev. Lett.* **85**, 5444 (2000).